

Polarized light scattering by microroughness and small defects in dielectric layers

Thomas A. Germer

*Optical Technology Division
National Institute of Standards and Technology
Gaithersburg, Maryland 20899*

Received August 11, 2000; revised manuscript received November 28, 2000, accepted December 1, 2000

The polarization of light scattered by the surface of a material contains information that can be used to identify the sources of that scatter. In this paper, theories for light scattering from interfacial roughness of a dielectric layer and from defects in that dielectric layer are reviewed. Methods for calculating the Mueller matrix or Stokes vector for scatter from multiple sources and for decomposing a Stokes vector into contributions from two non-depolarizing scattering sources are derived. The theories are evaluated for a specific sample and geometry. Results show that some incident polarizations are more effective than others at discriminating amongst scattering sources, with *s*-polarized light being least effective. The polarization of light scattered from interfacial roughness depends upon the relative roughness of the two interfaces and the degree of correlation between the two interfaces. The scattering from defects in the film depends upon the depth of the defect and differs from that from any one of the cases of interfacial roughness. Scattering from defects randomly distributed in the film and for small dielectric permittivity variations in the film are also calculated. Experimental results are presented for a 52 nm SiO₂ film thermally grown on microrough silicon.

1. INTRODUCTION

Measurements of the polarization of scattered light have been shown to enable the distinction amongst different scattering mechanisms for the case of a single interface.^{1–4} When light is directed onto a surface at an oblique angle with the electric field linearly polarized in the plane of incidence (*p*-polarized), boundary conditions force the direction of the electric field to differ on each side of the interface. The electric field just above the surface tends to be more normal to the surface, while the electric field below the surface tends to be more parallel to the surface. In the Rayleigh approximation, a very small sphere will polarize in a direction parallel to the applied electric field and radiate as if it were an antenna in that direction. Furthermore, particles above the surface sense a field that varies in direction, amplitude, and phase with distance from the surface.⁴ Scattering by small amounts of roughness behaves like a combination of the two: dipoles are induced by the electric field above the surface, which radiate from below the surface (or vice versa).⁵ The light scattered into directions out of the plane of incidence will have polarizations which are signatures of each mechanism.^{1–4}

Particle and defect detection on surfaces is often hampered by the presence of surface roughness.⁶ Understanding the sources of background signal allows instrumentation to be designed which minimizes the signal from such sources. Since the polarization from single interface mi-

roughness is defined by the geometry and the optical constants of the material and not the roughness function, a device can be built which collects light over most of the hemisphere, yet is blind to microroughness.⁷ Such a device can substantially improve the sensitivity for detecting particles and defects on rough surfaces. The application of such a technique for the inspection of materials with dielectric layers requires knowledge of the polarization of scattering from different sources, including interfacial roughness, for its success.⁴

The previous work on single interfaces has raised the question about whether polarized light scattering techniques can be applied to characterize defects and roughness in dielectric layers. Such layers are interesting technologically, as they are found ubiquitously in optics, microelectronics, data storage media, and information display systems. In this Article, we review theories for light scattering from a single dielectric layer and explore applications of those theories. We also discuss the scattering from multiple sources and describe how polarized light scattering can enable the quantification of two different scattering sources. The theory is applied to experimental data for a 52 nm SiO₂ layer thermally grown on silicon.⁸

In Sec. 2, we describe the theoretical treatment for scattering from interfacial roughness and Rayleigh defects in a film. Included in Sec. 2 is a method for treating multiple sources, maintaining all of the polarimetric information, and a method for decomposing a measured polarization state into the sum of two different non-depolarizing scattering sources. In Sec. 3, we apply the theory to a specific system consisting of a 52 nm SiO₂ layer grown on silicon, and we compare the model calculations to experimental data. Finally, the work will be summarized, and conclusions will be made, in Sec. 4.

2. THEORY

2.A. General Considerations

Figure 1 (top) shows the geometry used for this discussion. Plane wave polarized light of wavelength λ irradiates the surface at an incident angle θ_i in the plane defined by unit vectors $\hat{\mathbf{x}}$ and $\hat{\mathbf{z}}$. We are interested in determining the Jones or Mueller matrix for scattering into a direction defined by a polar angle θ_r and an azimuthal (out-of-plane) angle ϕ_r . Unit vectors $\hat{\mathbf{k}}_i$ and $\hat{\mathbf{k}}_r$ describe the directions of propagation of the incident and scattered light, respectively. The polarization of the incident electric field is described by its components along the $\hat{\mathbf{s}}_i$ and $\hat{\mathbf{p}}_i$ directions, where $\hat{\mathbf{s}}_i$ is a unit vector perpendicular to both $\hat{\mathbf{k}}_i$ and $\hat{\mathbf{z}}$, and $\hat{\mathbf{p}}_i = \hat{\mathbf{k}}_i \times \hat{\mathbf{s}}_i$. Likewise, the polarization of the electric field scattered into a particular direction is described by its components along the $\hat{\mathbf{s}}_r$ and $\hat{\mathbf{p}}_r$ unit vectors, defined in an analogous manner as $\hat{\mathbf{s}}_i$ and $\hat{\mathbf{p}}_i$. We say that light is *p*-polarized (*s*-polarized) when it is polarized with its electric field parallel to $\hat{\mathbf{p}}$ ($\hat{\mathbf{s}}$). Throughout this discussion, we omit the $\exp(-i\omega t)$ time dependence for all fields.

The scattering (Jones) matrix \mathbf{S} is defined as the relationship between the incident and scattered fields:

$$\begin{pmatrix} E_s^{\text{scat}} \\ E_p^{\text{scat}} \end{pmatrix} = \frac{\exp(ikR)}{R} \begin{pmatrix} S_{ss} & S_{ps} \\ S_{sp} & S_{pp} \end{pmatrix} \begin{pmatrix} E_s^{\text{inc}} \\ E_p^{\text{inc}} \end{pmatrix}, \quad (1)$$

where R is the distance from the scatterer to the detector, and $k = 2\pi/\lambda$. The equivalent intensity relationship can be expressed using the Stokes-Mueller representation, via the bidirectional reflectance distribution function (BRDF) \mathbf{F}_r ,

$$d\Phi_r = \mathbf{F}_r \Phi_i \cos\theta_r d\Omega, \quad (2)$$

where Φ_i is the incident Stokes power vector, and $d\Phi_r$ is the differential scattered Stokes power vector, and $d\Omega$ is the differential solid angle. The factor of $\cos\theta_r$ is customary for the definition of the BRDF.^{6,9} The Mueller matrix \mathbf{F}_r can be derived from the Jones matrix \mathbf{S} using an operation,¹⁰ given in the Appendix, which we will denote by

$$\mathbf{F}_r = \mathbf{M}(\mathbf{S})/(A \cos\theta_i \cos\theta_r), \quad (3)$$

where A is the illuminated area on the sample.¹⁰⁻¹²

A Stokes vector power Φ can be characterized by each of its elements Φ_j ($j = 0,1,2,3$). We find that it is convenient to express the polarization state by specifying the principal angle of the polarization ellipse, η , and various degrees of polarization. The principal angle η is given by

$$\eta = \arctan(\Phi_1, \Phi_2)/2, \quad (4)$$

where the two argument arc tangent, $\arctan(a,b)$, returns the arc tangent of b/a , taking into account in which quadrant the point (a,b) lies. The angle η is measured counterclockwise from the \hat{s} direction, viewing into the source. The total degree of polarization is

$$P = (\Phi_1^2 + \Phi_2^2 + \Phi_3^2)^{1/2} / \Phi_0, \quad (5)$$

the degree of linear polarization is

$$P_L = (\Phi_1^2 + \Phi_2^2)^{1/2} / \Phi_0, \quad (6)$$

and the degree of circular polarization is

$$P_C = \Phi_3 / \Phi_0. \quad (7)$$

Depolarization ($P < 1$) results from a polarization state that changes randomly either in time or in space. If $P_C = 1$, the light is left-hand-circularly polarized. The parameters Φ_0 , η , P_L , and P_C completely describe the polarization and intensity of the light. In fact, in a coordinate system rotated by an angle η from the $\hat{s} - \hat{\mathbf{p}}$ coordinate system, the Stokes vector is in the simple form

$$\Phi = \Phi_0 \times (1, P_L, 0, P_C)^T. \quad (8)$$

Likewise, the parameters Φ_0 , η , P_C , and P also completely describe the polarization and intensity, since $P_L^2 = P^2 - P_C^2$. The use of these parameters over the Stokes parameters follows from the work on single interfaces: Many scattering sources yield $P = 1$ or $P_C = 0$, so that η was a good indicator of mechanism, and stray light in the experiment tends to affect only the total degree of polarization P . The disadvantage of using these parameters is that they do not behave linearly and uncertainties vary depending upon their respective values. For example, when $P_C = 1$ or -1 , the value of η is not well-defined. However, we will continue to use the latter four parameters to characterize the intensity and polarization of scattered light.

In the following subsections, we will consider scattering from interfacial microroughness (Sec. 2.B.) and from film defects (Sec. 2.C.), present a formalism for including multiple scatter-

ing sources (Sec. 2.D.), and derive a method for decomposing a Stokes vector into the amplitudes and correlation function of two scattering sources (Sec. 2.E.).

2.B. Interfacial microroughness

Figure 1 (bottom) shows a cross section of the dielectric film, defining the dielectric constants ε_1 and ε_2 , the thickness τ , and the surface height functions Δz_1 and Δz_2 . (Later, in Sec. 2.C., we will consider the scattering from a defect located a distance d above the buried interface.) First-order vector perturbation theory has been very successful at describing the intensity and polarization of light scattered by small amounts of roughness.¹³ The zero-order, unperturbed ($\Delta z_1 = 0$ and $\Delta z_2 = 0$) fields are found from the solution of the well-known problem of reflection from a dielectric film. The first-order calculation consists of expanding the electric and magnetic fields on both sides of each interface and the local surface normal to first order in the surface height function $\Delta z_m(x, y)$ about its mean. The requirement that the tangential electric and magnetic fields be continuous across the boundary leads to relationships between zero-order and first-order fields. The theory self-consistently handles the multiple reflections that occur for both orders of the field. However, since it assumes that the film thickness is constant, it does not account for long-range non-conformal roughness, which has sufficient amplitude to substantially vary the local film thickness. In order for the theory to be valid, the modulations of the surface height functions, $\Delta z_m(x, y)$, must be much less than the wavelength, λ , and the surface slope must be much less than unity.

Elson described the solution to first-order vector perturbation theory for scattering from interfacial microroughness in a dielectric stack.^{13–17} Since Ref. 13 is very explicit about how to carry out that calculation, we will not repeat its lengthy solution. It is useful, however, to present the less general solutions for roughness of each interface of a single dielectric overlayer (three-phase model), which can be simplified considerably. For the buried interface (1), the scattering matrix elements are given by

$$S_{uv}^{(1)} = (4/\pi)(\varepsilon_1 - \varepsilon_2) \exp[i(q_{i2} + q_{r2} - q_{r3} - q_{i3})\tau] q_{r3} q_{i3} A^{1/2} \Delta Z_1(\mathbf{q}) s_{uv}^{(1)}, \quad (9)$$

($u, v = s, p$) where

$$s_{pp}^{(1)} = -\varepsilon_2 q_{i2} q_{r2} (\varepsilon_1 k_i k_r - \varepsilon_2 q_{i1} q_{r1} \cos \phi_r) / (\Gamma_{pi} \Gamma_{pr}), \quad (10a)$$

$$s_{ps}^{(1)} = \varepsilon_2 k q_{i2} q_{r2} q_{i1} \sin \phi_r / (\Gamma_{pi} \Gamma_{sr}), \quad (10b)$$

$$s_{sp}^{(1)} = \varepsilon_2 k q_{i2} q_{r2} q_{r1} \sin \phi_r / (\Gamma_{si} \Gamma_{pr}), \quad (10c)$$

$$s_{ss}^{(1)} = -k^2 q_{i2} q_{r2} \cos \phi_r / (\Gamma_{si} \Gamma_{sr}), \quad (10d)$$

$$\Gamma_{p\beta} = \varepsilon_2 F_{p\beta}^{(+)} q_{\beta 3} - F_{p\beta}^{(-)} q_{\beta 2}, \quad (11a)$$

$$\Gamma_{s\beta} = F_{s\beta}^{(+)} q_{\beta 3} - F_{s\beta}^{(-)} q_{\beta 2}, \quad (11b)$$

$$F_{p\beta}^{(\pm)} = \varepsilon_2 K_{\beta}^{(\mp)} q_{\beta 1} - \varepsilon_1 K_{\beta}^{(\pm)} q_{\beta 2}, \quad (12a)$$

$$F_{s\beta}^{(\pm)} = K_{\beta}^{(\mp)} q_{\beta 1} - K_{\beta}^{(\pm)} q_{\beta 2}, \quad (12b)$$

$$K_{\beta}^{(\pm)} = \exp(2iq_{\beta 2}\tau) \pm 1, \quad (13)$$

$q_{\beta j} = k(\varepsilon_j - \sin^2 \theta_{\beta})^{1/2}$, and $k_{\beta} = k \sin \theta_{\beta}$ ($\beta = i$ or r and $j = 1$ or 2). The Fourier transform of the roughness of the m -th interface is given by

$$\Delta Z_m(\mathbf{q}) = A^{-1/2} \int_A d^2\mathbf{r} \Delta z_m(\mathbf{r}) \exp[i\mathbf{q} \cdot \mathbf{r}], \quad (14)$$

where $\Delta z_m(\mathbf{r})$ is the surface height function of the m -th layer about its mean value, and the integration is carried out over the irradiated area A . The power spectral density (PSD) function is $\langle |\Delta Z_m(\mathbf{q})|^2 \rangle$, where the average is over an ensemble of realizations. The vector \mathbf{q} is the 2-d surface wavevector, related to the scattering directions by

$$q_x = k_r \cos \phi_r - k_i, \quad (15a)$$

$$q_y = k_r \sin \phi_r. \quad (15b)$$

For the exposed interface (2), the scattering matrix elements are given by

$$S_{uv}^{(2)} = (1/\pi)(\varepsilon_2 - 1)q_{r3}q_{i3} \exp[i(-q_{i3} - q_{r3})\tau] A^{1/2} \Delta Z_2(\mathbf{q}) s_{uv}^{(2)}, \quad (16)$$

where

$$s_{pp}^{(2)} = -(\varepsilon_2 k_i k_r F_{pi}^{(+)} F_{pr}^{(+)} - q_{i2} q_{r2} F_{pi}^{(-)} F_{pr}^{(-)} \cos \phi_r) / (\Gamma_{pi} \Gamma_{pr}), \quad (17a)$$

$$s_{ps}^{(2)} = -k q_{i2} F_{pi}^{(-)} F_{sr}^{(+)} \sin \phi_r / (\Gamma_{pi} \Gamma_{sr}), \quad (17b)$$

$$s_{sp}^{(2)} = -k q_{r2} F_{si}^{(+)} F_{pr}^{(-)} \sin \phi_r / (\Gamma_{si} \Gamma_{pr}), \quad (17c)$$

$$s_{ss}^{(2)} = -k^2 F_{si}^{(+)} F_{sr}^{(+)} \cos \phi_r / (\Gamma_{si} \Gamma_{sr}). \quad (17d)$$

The scattering matrix elements in Eqs. (9) and (16) depend upon the surface height functions of the respective interfaces only as a common multiplicative product. That is, the polarization state of the scattered light does not depend upon the surface height functions. Therefore, to first order, the scattering from a single rough interface will not depolarized light. Furthermore, the fields resulting from the scattering of each interface are independent of each other.

2.C. Rayleigh defect in a thin film

In this section, we present the results for a small spherical defect of radius a and dielectric constant ε_{sph} located between two interfaces a distance d above the lower interface (see Fig. 1). We assume that the defect is small enough that we can apply the Rayleigh approximation, and assume the scattered field from the defect does not interact with the defect a second time. The polarizability of the defect is then

$$\alpha = a^3 (\varepsilon_{\text{sph}} - \varepsilon_2) / (\varepsilon_{\text{sph}} + 2\varepsilon_2). \quad (18)$$

Using the approach outlined in Ref. 2, accounting for the existence of the two interfaces, we arrive at the scattering matrix elements

$$S_{uv}^{\text{def}} = 4\alpha \exp[i(q_{i2} + q_{r2})(\tau - d) - i(q_{i3} + q_{r3})\tau] \varepsilon_2^{3/4} q_{i3} q_{r3} s_{uv}^{\text{def}}(d) \quad (19)$$

where

$$s_{pp}^{\text{def}}(d) = (k_1 k_r G_{pi}^{(+)} G_{pr}^{(+)} - q_{i2} q_{r2} G_{pi}^{(-)} G_{pr}^{(-)} \cos \phi_r) / (\Gamma_{pi} \Gamma_{pr}), \quad (20a)$$

$$s_{ps}^{\text{def}}(d) = k q_{i2} G_{pi}^{(-)} G_{sr}^{(+)} \sin \phi_r / (\Gamma_{pi} \Gamma_{sr}), \quad (20b)$$

$$s_{sp}^{\text{def}}(d) = k q_{r2} G_{si}^{(+)} G_{pr}^{(-)} \sin \phi_r / (\Gamma_{si} \Gamma_{pr}), \quad (20c)$$

$$s_{ss}^{\text{def}}(d) = k^2 G_{si}^{(+)} G_{sr}^{(+)} \cos \phi_r / (\Gamma_{si} \Gamma_{sr}), \quad (20d)$$

$$G_{p\beta}^{(\pm)} = \varepsilon_2 L_{\beta}^{(\mp)} q_{\beta 1} - \varepsilon_1 L_{\beta}^{(\pm)} q_{\beta 2}, \quad (21a)$$

$$G_{s\beta}^{(\pm)} = L_{\beta}^{(\mp)} q_{\beta 1} - L_{\beta}^{(\pm)} q_{\beta 2}, \quad (21b)$$

$$L_{\beta}^{(\pm)} = \exp(2i q_{\beta 2} d) \pm 1. \quad (22)$$

The theory for scattering from variations in the permittivity of the film in the Rayleigh-Gans approximation follows from the theory above. Here, we assume that the dielectric constant of the material is given by $\varepsilon'_2 = \varepsilon_2 + \Delta\varepsilon_2(\mathbf{r})$, where $\Delta\varepsilon_2(\mathbf{r})$ is small and has zero mean, and the origin of \mathbf{r} is on interface 1. Recognizing that the differential polarizability is given by

$$d\alpha = \Delta\varepsilon_2 / (4\pi\varepsilon_2) d^3\mathbf{r}, \quad (23)$$

the scattering matrix is

$$S_{uv}^{\text{R-G}} = \exp[i(q_{i2} + q_{r2} - q_{i3} - q_{r3})\tau] \pi^{-1} \varepsilon_2^{-1/4} q_{i3} q_{r3} \int_V d^3\mathbf{r} \Delta\varepsilon_2(\mathbf{r}) s_{uv}^{\text{def}}(r_z) \exp[-i\mathbf{q}' \cdot \mathbf{r}], \quad (24)$$

where \mathbf{q}' is the 3-d scattering wavevector whose elements are given by

$$q'_x = k_r \cos \phi_r - k_1, \quad (25a)$$

$$q'_y = k_r \sin \phi_r, \quad (25b)$$

$$q'_z = q_{i2} + q_{r2}, \quad (25c)$$

and the integration is carried out over the volume of the film ($V = A\tau$) illuminated by the incident light. The scattering is therefore proportional to the 3-d Fourier transform of $\Delta\varepsilon_2(\mathbf{r}) s_{uv}^{\text{def}}(r_z)$.

2.D. Scattering from multiple sources

The field from different sources can add with some degree of coherence, which depends upon the phase correlation between those scattering sources. For n different partial fields, \mathcal{E}_m , the intensity is

$$I = \left\langle \left| \sum_{j=1}^n \mathcal{E}_m \exp(i\alpha_m) \right|^2 \right\rangle \quad (26)$$

where α_m is the phase associated with the m -th partial field ($m = 1 \dots n$), and the average is over an ensemble of realizations of the surface and the incident field, and over the collection solid angle. With a little bit of algebra, and assuming that amplitude and phase fluctuations are not correlated, Eq. (26) can be rewritten as

$$I = \sum_{m=1}^n I_m + \sum_{m=2}^n \sum_{m'=1}^{m-1} \left[(I_{mm'}^{(1)} - I_m - I_{m'}) \text{Re } c_{mm'} + (I_{mm'}^{(2)} - I_m - I_{m'}) \text{Im } c_{mm'} \right], \quad (27)$$

where $I_m = \langle |\mathcal{E}_m|^2 \rangle$ is the intensity of the m -th field alone, $I_{mm'}^{(1)} = \langle |\mathcal{E}_m + \mathcal{E}_{m'}|^2 \rangle$ is the intensity of two fields adding coherently in phase, $I_{mm'}^{(2)} = \langle |\mathcal{E}_m + i\mathcal{E}_{m'}|^2 \rangle$ is the intensity of two fields adding coherently but out of phase by $\pi/2$, and $c_{mm'} = \langle \exp[i(\alpha_m - \alpha_{m'})] \rangle$ is the degree of phase correlation between two fields. For two sources ($n = 2$), Eq. (27) can be written as

$$I = I_1 + I_2 + (I_{12}^{(1)} - I_1 - I_2) \text{Re } c_{12} + (I_{12}^{(2)} - I_1 - I_2) \text{Im } c_{12}. \quad (28)$$

We assumed a scalar field in deriving Eq. (27). However, for scattering matrices or field vectors, Eq. (27) still holds, provided we replace the intensities I_m , $I_{mm'}^{(1)}$, and $I_{mm'}^{(2)}$ by either their Mueller matrix equivalents [$I_m \rightarrow \langle \mathbf{M}(\mathbf{S}_m) \rangle$, $I_{mm'}^{(1)} \rightarrow \langle \mathbf{M}(\mathbf{S}_m + \mathbf{S}_{m'}) \rangle$, and $I_{mm'}^{(2)} \rightarrow \langle \mathbf{M}(\mathbf{S}_m + i\mathbf{S}_{m'}) \rangle$, where the scattering matrix for the m -th scattering source is \mathbf{S}_m] or their Stokes vector equivalents [$I_m \rightarrow \langle \boldsymbol{\Sigma}(\mathbf{E}_m) \rangle$, $I_{mm'}^{(1)} \rightarrow \langle \boldsymbol{\Sigma}(\mathbf{E}_m + \mathbf{E}_{m'}) \rangle$, and $I_{mm'}^{(2)} \rightarrow \langle \boldsymbol{\Sigma}(\mathbf{E}_m + i\mathbf{E}_{m'}) \rangle$, where the field vector for the m -th scattering source is \mathbf{E}_m]. Eq. (27) is very practical for determining the Mueller matrix for a combination of scattering sources where the degree of coherence between the sources is known. For example, in Subsection 2.B, we described the scattering from a single rough interface in the presence of other smooth interfaces. We can readily calculate the Mueller matrix BRDF for scattering from multiple rough interfaces, be their roughnesses correlated, uncorrelated, partially correlated, or even anti-correlated, by applying Eq. (27).

2.E. Decomposing a Stokes vector into two nondepolarizing sources

The scattering sources discussed in Secs. 2.B. and 2.C. above do not yield any depolarization when acting alone (assuming d is fixed in Sec. 2.C.). Therefore, it is possible to construct a physical device that is insensitive to any one of these scattering sources. Such a device uses an appropriately aligned retarder and polarizer in front of a detector to null the signal from a specific source. This principle has been used to develop microroughness-blind instrumentation designed to improve sensitivity to defects in the presence of a dominating background signal from microroughness.⁷ Using this principle, we develop a mathematical method to decompose an arbitrary Stokes vector into a combination of two scattering fields, that is, developing a means to invert Eq. (28).

If the scattering Stokes vector intensity from a specific source is $\boldsymbol{\Psi} = (\psi_0, \psi_1, \psi_2, \psi_3)^T$, and if $\boldsymbol{\Psi}$ has a degree of polarization $P = 1$ (i.e., $\psi_0^2 = \psi_1^2 + \psi_2^2 + \psi_3^2$), then we can construct a Stokes vector sensitivity $\bar{\boldsymbol{\Psi}} = (\psi_0, -\psi_1, -\psi_2, -\psi_3)^T$ such that $\bar{\boldsymbol{\Psi}}^T \boldsymbol{\Psi} = 0$. That is, a detector having Stokes vector sensitivity proportional to $\bar{\boldsymbol{\Psi}}$ will be blind to a source scattering with Stokes vector proportional to $\boldsymbol{\Psi}$.

Assume that we measure a Stokes vector intensity $\boldsymbol{\Phi}$ in a specific geometry. We would like to decompose $\boldsymbol{\Phi}$ into the sum of two (and *only* two) non-depolarizing scattering sources, each of which yield Jones matrices $\kappa_1 \mathbf{J}_1$ and $\kappa_2 \mathbf{J}_2$, respectively. It is assumed that we can calculate \mathbf{J}_1 and \mathbf{J}_2 , but that we do not know the scaling parameters κ_1 and κ_2 . The respective Stokes vector representations for \mathbf{J}_1 and \mathbf{J}_2 are $\boldsymbol{\Psi}_1 = \boldsymbol{\Sigma}(\mathbf{J}_1)$ and $\boldsymbol{\Psi}_2 = \boldsymbol{\Sigma}(\mathbf{J}_2)$. Stokes vectors $\hat{\boldsymbol{\Psi}}_1 = \bar{\boldsymbol{\Psi}}_2 / (\bar{\boldsymbol{\Psi}}_2^T \boldsymbol{\Psi}_1)$ and $\hat{\boldsymbol{\Psi}}_2 = \bar{\boldsymbol{\Psi}}_1 / (\bar{\boldsymbol{\Psi}}_1^T \boldsymbol{\Psi}_2)$ can be constructed such that $\hat{\boldsymbol{\Psi}}_j^T \boldsymbol{\Psi}_{j'} = \delta_{jj'}$ ($j, j' = 1, 2$). It is then straightforward to show that the magnitudes of the scaling factors for \mathbf{J}_1 and \mathbf{J}_2 are given by

$$|\kappa_1| = (\hat{\Psi}_1^T \Phi)^{1/2}, \quad (29a)$$

$$|\kappa_2| = (\hat{\Psi}_2^T \Phi)^{1/2}. \quad (29b)$$

We can now define $\Psi_{12}^{(1)} = \Sigma(|\kappa_1| \mathbf{J}_1 + |\kappa_2| \mathbf{J}_2)$ and $\Psi_{12}^{(2)} = \Sigma(|\kappa_1| \mathbf{J}_1 + i|\kappa_2| \mathbf{J}_2)$, and construct $\bar{\Psi}_{12}^{(1)}$ and $\bar{\Psi}_{12}^{(2)}$ as above. Applying $\bar{\Psi}_{12}^{(1)T}$ and $\bar{\Psi}_{12}^{(2)T}$ each to Eq. (28) yields the system of equations:

$$b_1 = a_{11} \operatorname{Re} c_{12} + a_{12} \operatorname{Im} c_{12}, \quad (30a)$$

$$b_2 = a_{21} \operatorname{Re} c_{12} + a_{22} \operatorname{Im} c_{12}, \quad (30b)$$

where

$$a_{jj'} = \bar{\Psi}_{12}^{(j)T} (\Psi_{12}^{(j')} - |\kappa_1|^2 \Psi_1 - |\kappa_2|^2 \Psi_2), \quad (31a)$$

$$b_j = \bar{\Psi}_{12}^{(j)T} (\Phi - |\kappa_1|^2 \Psi_1 - |\kappa_2|^2 \Psi_2). \quad (31b)$$

Eqs. (30) can then be solved for c_{12} :

$$\operatorname{Re} c_{12} = (a_{12} b_2 - a_{22} b_1) / (a_{21} a_{12} - a_{11} a_{22}), \quad (32a)$$

$$\operatorname{Im} c_{12} = (a_{21} b_1 - a_{11} b_2) / (a_{21} a_{12} - a_{11} a_{22}). \quad (32b)$$

Eqs. (29), (31), and (32) can be used to extract the relative quantities and phase correlations for two scattering sources from measured Stokes vector intensity data.

3. RESULTS AND DISCUSSION

To demonstrate the results of the models presented in Sec. 2, we consider the calculated behavior of $\lambda = 632.8$ nm light scattered by a 52 nm SiO₂ ($\epsilon_2 = 2.13$) layer grown on a silicon ($\epsilon_1 = 15.07 + 0.15i$) substrate. These conditions were chosen to match those of a specific sample, from which measurements were performed. We further chose to limit our discussion to an incident angle of $\theta_i = 60^\circ$ and scattering angle $\theta_r = 60^\circ$. When $\theta_i = \theta_r$, the spatial wavevectors probed have magnitude $|\mathbf{q}| = 2k \sin \theta_i \sin(\phi_r / 2)$.

Figure 2 shows the polarization state as a function of ϕ_r for four different incident polarization schemes and for four different limiting cases of interfacial roughness (roughness of each interface and correlated and uncorrelated roughness). The results for s -polarized incident light (leftmost column of Fig. 2) show only a small amount of differentiation between the roughness conditions, with none existing at $\phi_r = 0^\circ, 90^\circ$, and 180° . For a single interface, previous work demonstrated that small spheres above and in contact with that interface, small spheres below that interface, and microroughness yield identical scattered light polarizations with s -polarized incident light.² In fact, symmetry dictates the polarization for $\phi_r = 0^\circ, 90^\circ$, and 180° : For s -polarized light incident upon an isotropic sample in the static approximation, the scattered field must be anti-symmetric about the x - z plane and symmetric about the y - z plane. Therefore, in the plane of incidence ($\phi_r = 0^\circ$ and 180°), the scattered light must be s -polarized ($s_{sp} = s_{ps} = 0$), while for $\phi_r = 90^\circ$, the scattered light must be p -polarized ($s_{ss} = 0$).

The results for p -polarized incident light (second column in Fig. 2) show a significantly greater differentiation between the different scattering sources, as long as one is sufficiently out of the plane of incidence ($\phi_r \neq 0^\circ$ or 180°). Again, symmetry requires that the scattered light be p -

polarized in the plane of incidence. However, no symmetry exists about the y - z plane for p -polarized incident light, so that for $\phi_t = 90^\circ$, each mechanism can yield a different polarization ($s_{pp} \neq 0$). Previous measurements have exploited this geometry for scattering from small particles, single rough surfaces, and subsurface defects.^{1,3,4} However, in measurements of roughness, one is often interested in extracting roughness statistics from data over as wide a spatial frequency range as possible.⁶ Since there is little differentiation between mechanisms near $\phi_t = 0^\circ$, the dynamic range of available spatial frequencies is limited.

The third and fourth columns of Fig. 2 present alternative schemes which allow differentiation between different interfacial roughness conditions for most scattering angles. The simplest of these schemes is to use circularly polarized incident light (third column of Fig. 2). A more complicated scheme involves changing the incident polarization state as the viewing direction is varied. In the fourth column of Fig. 2, the incident light is linearly polarized with a direction given by $\eta_i = 45^\circ + \phi_t / 2$. Reasonably good differentiation between the different roughness conditions can be observed at most scattering angles, using the two schemes, with somewhat better differentiation observed for the varying incident polarization scheme.

The results for polarized light scattering measurements from a 52 nm SiO_2 film thermally grown on a photolithographically-produced microrough silicon surface are included in Fig. 2. The microrough surface consisted of a pseudorandom distribution of 8 nm deep circular pits having diameters of 1.31 μm and 1.76 μm . Details of the experiment, its uncertainties, and the sample are given elsewhere.^{8,18} This system should exhibit conformal roughness, at least for small spatial frequencies. The results shown in Fig. 2 indeed behave most like the equal roughness model for all incident polarizations, though close inspection of the results reveals small discrepancies, which result from the buried interface being smoother than the exposed interface. The relative roughness of the two interfaces (Z_2/Z_1) and the degree of correlation c_{12} can be extracted using the technique outlined in Sec. 2.E.⁸ Figure 3 shows c_{12} and Z_2/Z_1 as functions of spatial frequency extracted from the data shown in three of the columns in Fig. 2. The indicated uncertainties represent single standard deviations of the extracted results obtained from the statistical uncertainties in the original data. The results obtained from all incident polarizations are consistent with each other, showing $Z_2/Z_1 > 1$ and $c_{12} \sim 1$ for most spatial frequencies. Further validation of the method has been achieved by performing the measurements at multiple wavelengths and incident angles.⁸

While measurements of the full Mueller matrix may allow different scattering mechanisms to be distinguished and quantified using the analysis given in Sec. 2.D., the results shown in Fig. 2 suggest that certain incident polarization states don't allow for much differentiation. If this is the case, the Mueller matrix formalism may not be an efficient means for identifying scattering sources. That is, figuratively speaking, there are more elements to the Mueller matrix than the number of degrees of freedom spanned by the available models. An extreme example of this principle can be found in the plane of incidence, for which there are only six degrees of freedom to the Mueller matrix. In this case, measuring all sixteen elements will not yield more information about the scattering source than measuring six independent nonzero elements. For that reason, we have focussed our attention on measurements of the Stokes vector for incident polarization states chosen to maximize source differentiation. While we are offering specific schemes, they may not be truly optimal for all samples.

Figure 4 shows the calculated results for the different roughness conditions evaluated in the plane of incidence ($\theta_i = 60^\circ$, $\phi_t = 0^\circ$), together with results obtained from the 52 nm SiO_2/Si sample. Since the scattering matrices are diagonal for this geometry, we do not show results for s -

polarized or p -polarized incident light. Incident light of either circular polarization or linear polarization along the $\hat{s}_i - \hat{p}_i$ direction maps the four independent Mueller matrix elements onto the four Stokes vector elements. While discrimination between roughness conditions can be observed in Fig. 4, it is relatively weak, with numerous curves crossing near $\theta_r = 15^\circ$. Figure 3 includes the results of the analysis described in Sec. 2.E. using the data obtained in the plane of incidence. Large uncertainties and discrepancies result from the poor discrimination near $1 \mu\text{m}^{-1}$. Comparison between the results of Figs. 2 and 4 suggest that maximum discrimination between different roughness conditions occurs in directions out of the plane of incidence. Other calculations show that such improvements also tend to occur for other scattering sources such as particles or subsurface defects. While other researchers have performed light scattering ellipsometry measurements in the plane of incidence,¹⁹ we chose to make full use of the polarization by performing such measurements in out-of-plane geometries.

It is noteworthy to point out that in all of the columns of Figs. 2 and 4, the results for buried interface roughness and uncorrelated roughness are the most poorly resolved. In both cases, the roughness of the bottom interface is present, and the top interface is incoherent with the bottom interface. When sources are incoherent, they add as intensities, rather than fields, so that the smaller field has a correspondingly smaller effect. Hence, when the dielectric contrast between the substrate and the film is much larger than between film and the ambient environment, which is the case for our example, uncorrelated roughness of the top interface will be more difficult to observe in the presence of buried interface roughness.

Figure 5 shows results using the varying-incident-polarization scheme for scattering from six different individual sources: from each of the two interfaces alone and from four Rayleigh defects, positioned just above and below each interface. Since each of the curves in Fig. 5 represents a single mechanism, there are no sources of depolarization ($P = 1$). Each scattering source shown in Fig. 5 yields a different polarization state for every scattering direction. The differences between the curves in Fig. 5 are sufficiently great that a measurement system with a 1° resolution in η and a 0.01 resolution in P_C and P should be able to distinguish amongst them.

The difference between the results for cases (c) and (d) in Fig. 5, corresponding to defects in extreme locations of the film, suggests there is a dependence of the polarization of the scattered light on the position of the scatterer within the film. Figure 6 shows that dependence for the geometry $\theta_i = \theta_r = 60^\circ$ and $\phi_r = 90^\circ$. For thicker films, oscillations in polarization and intensity of period $l = \lambda q_{12} / (2k)$ can be observed, which result from interference between each interface. The properties of the scattered light do not depend upon depth in the bulk material, since no interference between reflected waves exists; if the substrate material were absorbing, the intensity would decay as the depth increased.

If a large number of defects exist in the dielectric film within the illuminated region, then only under specific conditions would they all have a single value of d . If they are randomly distributed in the layer with no correlations, we can integrate the Mueller matrix over the layer to arrive at an incoherently-summed net Mueller matrix. Figure 7 shows the dependence of the layer average on ϕ_r for defects in the dielectric layer. While there are many functional forms imaginable for dielectric permittivity variations in a dielectric film, one is particularly easy to calculate and of some interest: $\epsilon_2(x, y, z) = \epsilon_2(x, y, 0)$. This functional form corresponds to that of columnar growth or columnar phase separation between two similar materials. The calculated results for such a material are shown in Fig. 7, and can be seen to differ from that of random defects in the film. The results for roughness of the exposed interface are also included in Fig. 7. Columnar

variations in permittivity yield very similar polarizations to those obtained from roughness of the exposed interface (remember that when $|P_C|$ is near 1, the value of η is not well defined), and this poor discrimination exists for a relatively wide range of film thicknesses and incident angles. Films having such morphology would likely exhibit coherent surface roughness of the top interface, and quantifying the two effects may prove difficult using the techniques outlined here.

The strong dependence of the polarization of the scattered light for particles outside of the material (see Fig. 6) has a potentially powerful application. Generally speaking, the intensity of light scattered by a particle (when it is sufficiently small) provides insufficient information to determine both its size and its material. The interference behavior outside of the material suggests that a larger particle can be distinguished from a smaller one by the polarization of the scattered light, since the size of a particle determines its mean distance from the surface. This result is not dependent upon the existence of the dielectric layer, but relies instead upon interference between the incident and reflected light outside of the material. Measurements demonstrating this behavior, and calculations with more accurate models, are presented elsewhere.^{4,20}

In order to keep this article to a reasonable length, we chose not to discuss features that can be observed in the scattered light intensity, except in so far as was needed to show that interference exists in the film. Numerous other studies have discussed the intensity of light scattered by defects in or near thin films,^{14,21–24} and it is our motivation to illustrate that information contained in the polarization is useful for distinguishing amongst different scattering sources. Certainly, measurement of intensity is important for classifying the scattering properties of defects. For example, for roughness, the intensity is required to obtain roughness statistics.

Although we chose to study a particular system, the models are applicable to a wide range of different materials, including different dielectrics and thicknesses on silicon, coatings on transparent or reflecting optics, and protective coatings on materials. For most of these systems, provided that the optical constants of the materials involved are known, an equivalent set of results will be obtained.

4. SUMMARY AND CONCLUSIONS

In this paper, we have reviewed models for polarized light scattering from interfacial roughness and small spherical defects in a dielectric layer. Furthermore, we have derived an expression for the Stokes vector when a number of scattering sources exist and when the degree of correlation between those sources is known. We have also derived an algorithm for inverting that expression, allowing a Stokes vector to be decomposed into the superposition of two non-depolarizing sources. To illustrate the application of these models, we consider a specific system consisting of a 52 nm SiO₂ layer on silicon. We find that scattering from each of six sources, roughness at each of the two interfaces and Rayleigh scattering above and below each interface, gives rise to a unique behavior for the polarization. We show how light scattering from defects depends upon the position of the defect in the layer, and evaluated the ellipsometric parameters for a random distribution of defects in the layer and for a columnar morphology. We consider the scattering from roughness at both interfaces and find that the results were strongly dependent upon the correlation of the roughness, showing that measurements of the polarization of scattered light could be used to determine the roughness and cross-correlation functions of two interfaces. The methods described in this paper are used to determine the relative roughness of the two interfaces of a 52 nm SiO₂ layer thermally grown on silicon. We compare different scattering geometries and find that measurements of the Stokes parameters out of the plane of incidence for

specific (but not necessarily fixed) incident polarizations yielded the strongest discrimination amongst different scattering sources.

The technique of light scattering ellipsometry should prove useful for analyzing light scattered by systems with dielectric layers. In many situations, the location of a scattering source can be determined. This capability should be useful for rapid analysis of materials, such as is needed for on-line quality control inspection of computer disks, semiconductor wafers, and flat panel displays, and for high throughput screening of combinatorial libraries.

Appendix A

The Stokes vector equivalent of a Jones vector \mathbf{J} can be expressed by the function $\Sigma(\mathbf{J})$. The elements of the Stokes vector returned by $\Sigma(\mathbf{E})$ are:

$$\Sigma_0 = (\epsilon_0 / \mu_0)^{1/2} (|J_s|^2 + |J_p|^2), \quad (\text{A.1a})$$

$$\Sigma_1 = (\epsilon_0 / \mu_0)^{1/2} (|J_s|^2 - |J_p|^2), \quad (\text{A.1b})$$

$$\Sigma_2 = 2(\epsilon_0 / \mu_0)^{1/2} \text{Re}(J_s^* J_p), \quad (\text{A.1c})$$

$$\Sigma_3 = 2(\epsilon_0 / \mu_0)^{1/2} \text{Im}(J_s^* J_p). \quad (\text{A.1d})$$

The conversion from a Jones scattering matrix S to a Mueller Matrix has been represented in this article by a function $\mathbf{M}(\mathbf{S})$. This transformation is given explicitly here for reference. The elements of the Mueller matrix returned by $\mathbf{M}(\mathbf{S})$ are

$$m_{00} = (|S_{pp}|^2 + |S_{ss}|^2 + |S_{sp}|^2 + |S_{ps}|^2) / 2 \quad (\text{A.2a})$$

$$m_{01} = (|S_{ss}|^2 - |S_{pp}|^2 + |S_{sp}|^2 - |S_{ps}|^2) / 2 \quad (\text{A.2b})$$

$$m_{02} = \text{Re}(S_{ss} S_{ps}^* + S_{pp} S_{sp}^*) \quad (\text{A.2c})$$

$$m_{03} = \text{Im}(S_{ss} S_{ps}^* - S_{pp} S_{sp}^*) \quad (\text{A.2d})$$

$$m_{10} = (|S_{ss}|^2 - |S_{pp}|^2 - |S_{sp}|^2 + |S_{ps}|^2) / 2 \quad (\text{A.2e})$$

$$m_{11} = (|S_{ss}|^2 + |S_{pp}|^2 - |S_{sp}|^2 - |S_{ps}|^2) / 2 \quad (\text{A.2f})$$

$$m_{12} = \text{Re}(S_{ss} S_{ps}^* - S_{pp} S_{sp}^*) \quad (\text{A.2g})$$

$$m_{13} = \text{Im}(S_{ss} S_{ps}^* + S_{pp} S_{sp}^*) \quad (\text{A.2h})$$

$$m_{20} = \text{Re}(S_{ss} S_{sp}^* + S_{pp} S_{ps}^*) \quad (\text{A.2i})$$

$$m_{21} = \text{Re}(S_{ss} S_{sp}^* - S_{pp} S_{ps}^*) \quad (\text{A.2j})$$

$$m_{22} = \text{Re}\left(S_{pp}S_{ss}^* + S_{ps}S_{sp}^*\right) \quad (\text{A.2k})$$

$$m_{23} = \text{Im}\left(S_{ss}S_{pp}^* + S_{sp}S_{ps}^*\right) \quad (\text{A.2l})$$

$$m_{30} = \text{Im}\left(S_{sp}S_{ss}^* + S_{pp}S_{ps}^*\right) \quad (\text{A.2m})$$

$$m_{31} = \text{Im}\left(S_{sp}S_{ss}^* - S_{pp}S_{ps}^*\right) \quad (\text{A.2n})$$

$$m_{32} = \text{Im}\left(S_{pp}S_{ss}^* - S_{ps}S_{sp}^*\right) \quad (\text{A.2o})$$

$$m_{33} = \text{Re}\left(S_{pp}S_{ss}^* - S_{ps}S_{sp}^*\right) \quad (\text{A.2p})$$

REFERENCES

1. T. A. Germer, C. C. Asmail, and B. W. Scheer, "Polarization of out-of-plane scattering from microrough silicon," *Opt. Lett.* **22**, 1284-1286 (1997).
2. T. A. Germer, "Angular dependence and polarization of out-of-plane optical scattering from particulate contamination, subsurface defects, and surface microroughness," *Appl. Opt.* **36**, 8798-8805 (1997).
3. T. A. Germer and C. C. Asmail, "Polarization of light scattered by microrough surfaces and subsurface defects," *J. Opt. Soc. Am. A* **16**, 1326-1332 (1999).
4. L. Sung, G. W. Mulholland, and T. A. Germer, "Polarized light-scattering measurements of dielectric spheres upon a silicon surface," *Opt. Lett.* **24**, 866-868 (1999).
5. E. Kröger and E. Kretschmann, "Scattering of light by slightly rough surfaces or thin films including plasma resonance emission," *Z. Physik* **237**, 1-15 (1970).
6. J. C. Stover, *Optical Scattering: Measurement and Analysis*, (SPIE Optical Engineering Press, Bellingham, WA, 1995).
7. T. A. Germer and C. C. Asmail, "Microroughness-blind optical scattering instrument," United States Patent #6,034,776 (Mar. 7, 2000).
8. T. A. Germer, "Measurement of roughness of two interfaces of a dielectric film by scattering ellipsometry," *Phys. Rev. Lett.* **85**, 349-352 (2000).
9. F. E. Nicodemus, J. C. Richmond, J. J. Hsia, I. W. Ginsberg, and T. Limperis, "Geometrical Considerations and Nomenclature for Reflectance," NBS Monograph 160, (National Bureau of Standards, Gaithersburg, 1977).
10. C. F. Bohren and D. R. Huffman, *Absorption and Scattering of Light by Small Particles*, (Wiley, New York, 1983).
11. H. C. van de Hulst, *Light Scattering by Small Particles*, (Dover, New York, 1981).

12. D. S. Flynn and C. Alexander, "Polarized surface scattering expressed in terms of a bidirectional reflectance distribution function matrix," *Opt. Eng.* **34**, 1646-1650 (1995).
13. J. M. Elson, "Multilayer-coated optics: guided-wave coupling and scattering by means of interface random roughness," *J. Opt. Soc. Am. A* **12**, 729-742 (1995).
14. J. M. Elson, J. P. Rahn, and J. M. Bennett, "Light scattering from multilayer optics: comparison of theory and experiment," *Appl. Opt.* **19**, 669-679 (1980).
15. J. M. Elson, "Diffraction and diffuse scattering from dielectric multilayers," *J. Opt. Soc. Am.* **69**, 48-54 (1979).
16. J. M. Elson, "Infrared light scattering from surfaces covered with multiple dielectric overlayers," *Appl. Opt.* **16**, 2873-2881 (1977).
17. J. M. Elson, "Light scattering from surfaces with a single dielectric overlayer," *J. Opt. Soc. Am.* **66**, 682-694 (1976).
18. T. A. Germer and C. C. Asmail, "Goniometric optical scatter instrument for out-of-plane ellipsometry measurements," *Rev. Sci. Instr.* **70**, 3688-3695 (1999).
19. C. Deumiè, H. Giovannini, and C. Amra, "Ellipsometry of light scattering from multilayer coatings," *Appl. Opt.* **35**, 5600-5608 (1996).
20. L. Sung, G. W. Mulholland, and T. A. Germer, "Polarization of light scattered by spheres on a dielectric film," in *Rough Surface Scattering and Contamination*, P.-T. Chen, Z.-H. Gu, and A. A. Maradudin, Eds., *Proc. SPIE*, **3784**, 296-303 (1999).
21. D. Rönnow, "Interface roughness statistics of thin films from angle-resolved light scattering at three wavelengths," *Opt. Eng.* **37**, 696-704 (1998).
22. C. Amra, C. Grèzes-Besset, and L. Bruel, "Comparison of surface and bulk scattering in optical multilayers," *Appl. Opt.* **32**, 5492-5503 (1993).
23. C. Amra, "First-order vector theory of bulk scattering in optical multilayers," *J. Opt. Soc. Am. A* **10**, 365-374 (1993).
24. S. Kassam, A. Duparrè, K. Hehl, P. Bussemer, and J. Neubert, "Light scattering from the volume of optical thin films: theory and experiment," *Appl. Opt.* **31**, 1304-1313 (1992).

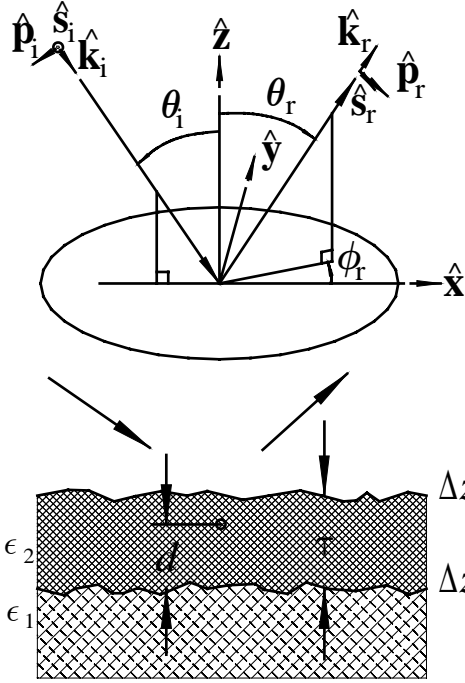


Fig. 1. (top) The scattering and sample coordinate system, and (bottom) a diagram showing the thin film with a embedded defect.

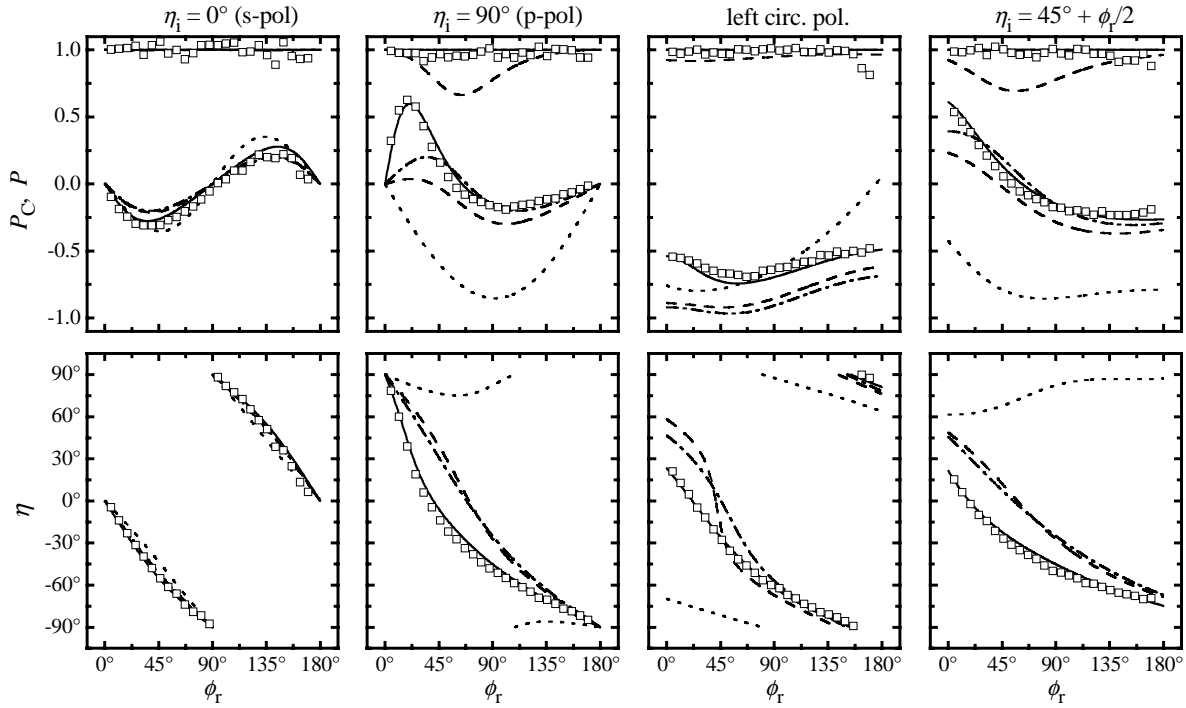


Fig. 2. Polarization parameters P_C , P , and η for scattering out of the plane of incidence from (solid) correlated and equal roughness, (dashed) uncorrelated and equal roughness, (dotted) roughness of the exposed interface, (dash-dot) roughness of the buried interface, and (symbols) experimental results from a SiO_2 layer grown on microrough silicon. Each column refers to a different incident polarization scheme. Other parameters in the model are described in the text.

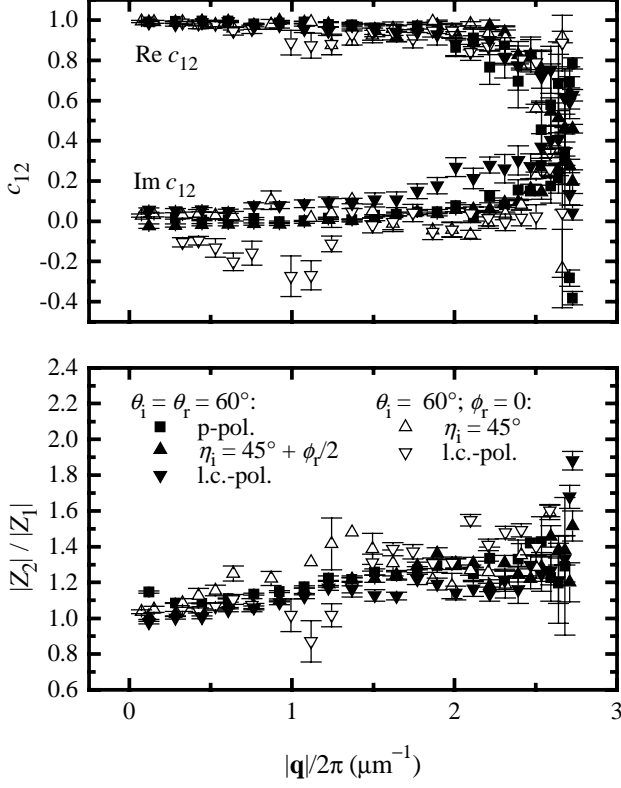


Fig. 3. Roughness parameters extracted from polarized light scattering measurements from the 52 nm SiO_2 layer thermally grown on silicon. The results are obtained from measurements out of the plane of incidence (solid symbols) and in the plane of incidence (open symbols).

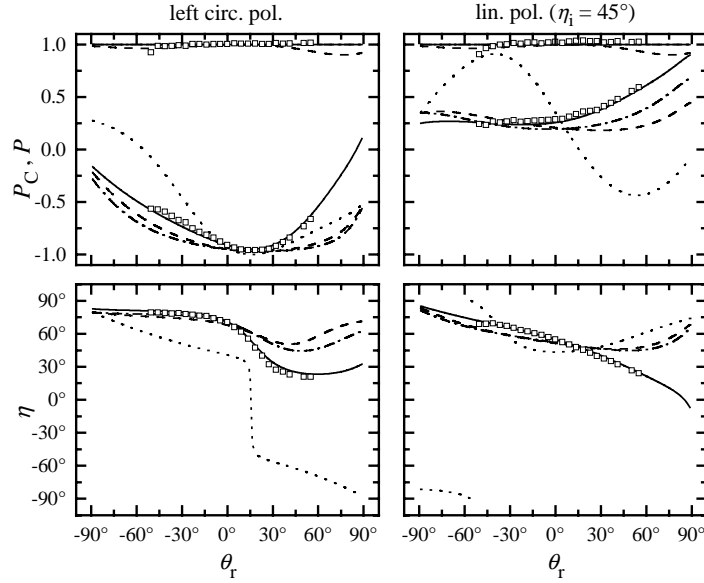


Fig. 4. Polarization parameters P_C , P , and η for scattering in the plane of incidence from (solid) correlated and equal roughness, (dashed) uncorrelated and equal roughness, (dotted) roughness of the exposed interface, (dash-dot) roughness of the buried interface, and (symbols) experimental results from a SiO_2 layer grown on microrough silicon. The incident polarizations were (left column) left circularly polarized and (right column) linearly polarized along the direction $\hat{\mathbf{s}}_i - \hat{\mathbf{p}}_i$

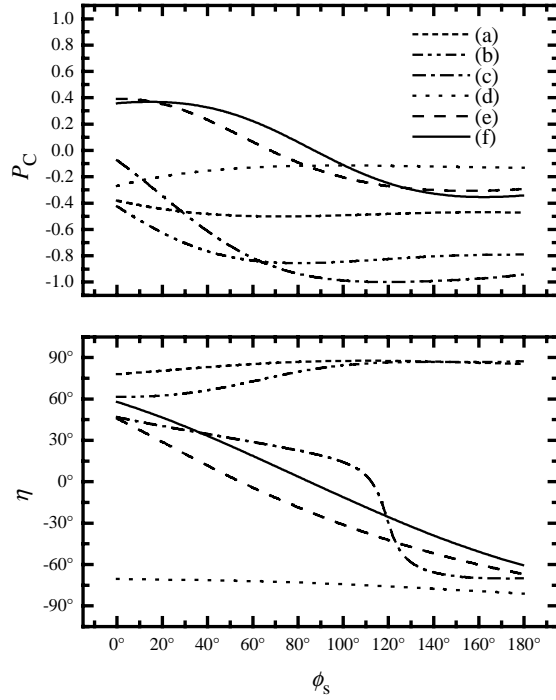


Fig. 5. Polarization parameters P_C , P , and η for scattering from different locations in the film, using the variable incident polarization scheme described in the text. The defects are (a) a Rayleigh defect just above the film, (b) roughness of the air/film interface, (c) a Rayleigh defect just below the air/film interface, (d) a Rayleigh defect just above the film/substrate interface, (e) roughness of the film/substrate interface, and (f) a Rayleigh defect in the substrate.

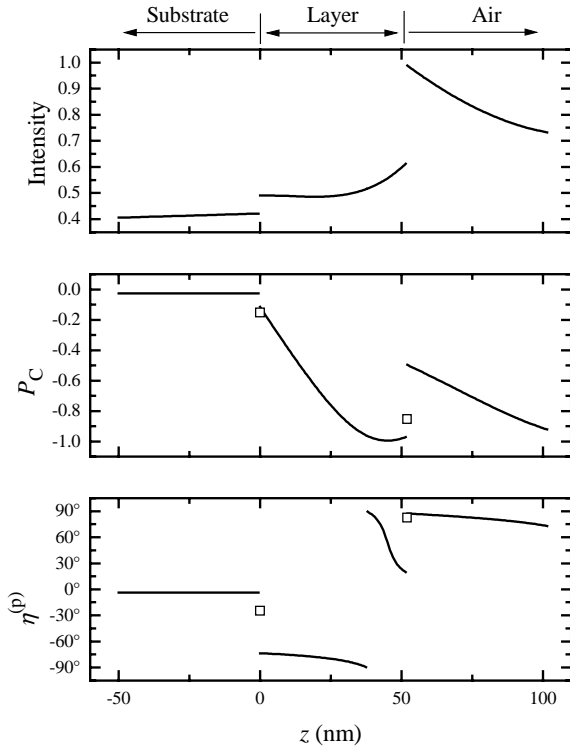


Fig. 6. The intensity, P_C , and η for scattering from different locations near the dielectric film. The incident and scattering angles are $\theta_i = \theta_r = 60^\circ$ and the out-of-plane angle is $\phi_r = 90^\circ$. The curves represent the positional dependence of a Rayleigh scatterer, while the symbols represent roughness at one of each of the two interfaces. The relative scales for the intensity are arbitrary between each layer.

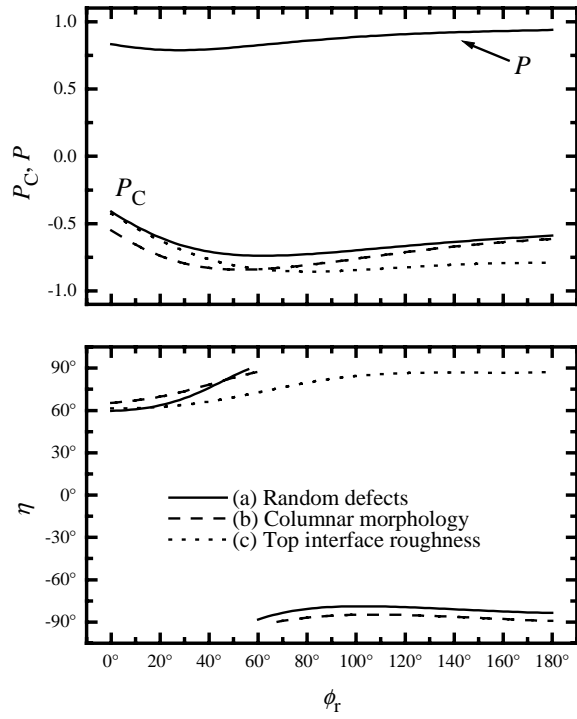


Fig. 7. Polarization parameters P_C , P , and η for scattering (solid curve) from a random distribution of Rayleigh defects in the film, and (dashed curve) from small variations in the dielectric permittivity of the film for which $\epsilon_2(x, y, d) = \epsilon_2(x, y, 0)$.